

Phase-Shifting Zernike Interferometer Wavefront Sensor

J. Kent Wallace*, Shanti Rao, Rebecca M. Jensen-Clem
Jet Propulsion Laboratory, California Institute of Technology, 4800 Oak Grove Drive,
Pasadena, CA, USA 91109;

ABSTRACT

The canonical Zernike phase-contrast technique transforms a phase object in one plane into an intensity object in the conjugate plane. This is done by applying a static $\pi/2$ phase shift to the central core ($\sim \lambda/D$) of the PSF which is intermediate between the input and output plane. Here we present a new architecture for this sensor. First, the optical system is simple and all reflective, and second the phase shift in the central core of the PSF is dynamic and can be made arbitrarily large. This common-path, all-reflective design makes it minimally sensitive to vibration, polarization and wavelength. We review the theory of operation, describe the optical system, summarize numerical simulations and sensitivities and review results from a laboratory demonstration of this novel instrument.

Keywords: Wavefront sensing, Zernike phase-contrast, adaptive optics.

1. INTRODUCTION

Zernike's method of phase-contrast was transformative for the biological sciences for it allowed biological specimens in aqueous solutions to be viewed for the first time not as intensity objects, but instead as phase objects. The amplitude of the light passing through these essentially transparent media (the aqueous solution and the cells, or instance) was unaffected and thus the specimen was indistinguishable from its surroundings. However, the index of refraction is distinctly different, and phase-contrast permitted these phase objects to be viewed as intensity objects. It is for this work that he was awarded the Nobel prize in 1953.

Dicke first proposed that the phase-contrast method could be employed for wavefront sensing in an adaptive optics system. In a similar manner, the index of refraction variations of the turbulent atmosphere leave the electric field amplitude primarily unaffected but create large phase errors. A Zernike wavefront sensor (ZWFS) would turn the phase errors into easily measured amplitude errors. But the Zernike wavefront sensor has other distinct advantages. For instance, the ZWFS measures the electric field phase directly. In comparison, the Shack-Hartmann wavefront sensor (SHWFS) reconstructs the phase by first measuring the phase gradient and then numerically integrating it. This process is susceptible to noise propagation, particularly in the lowest spatial frequency modes. The ZWFS, because it measures phase directly, does not suffer from this problem.

However, the classical static Zernike has other limitations. Given that the intensity of the output pupil is interpreted as phase, any noise source that generates an intensity measurement error will lead to an erroneous estimate of the phase. For instance, any light that is scattered (like a glint internal to the optical train) would lead to an intensity variation which in turn would be misinterpreted as phase in the input pupil. In the new architecture the static phase shift (say $\pi/2$) in the PSF is replaced by a dynamic and variable phase shift (nominally $-\pi/2$, 0 , $+\pi/2$, and $+\pi$). This diversity in the phase allows the intensity images to be demodulated such that the phase and amplitude of the electric field can be determined independently. Likewise, any part of the intensity measurement that is not also modulated by these phase shifts is rejected in the reconstruction process which makes the sensor insensitive to issues such as scattered light and glints as well as noise sources in the detection process (like detector noise) that is not synchronous with the phase modulation.

2. PRINCIPLES OF ZERNIKE PHASE CONTRAST

The following discussion of Zernike phase contrast can be found in many optical textbooks. The purpose of including it here is to demonstrate the simplicity with which the phase can be reconstructed using the dynamic Zernike WFS. The input pupil, image plane, and output pupil, refer to the canonical optical system represented in Figure 1.

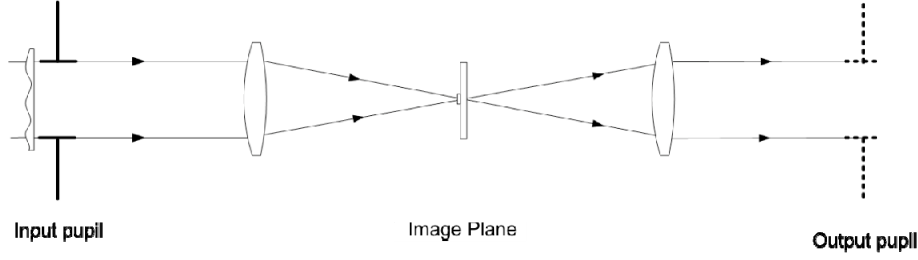


Figure 1. The canonical optical system used to illustrate Zernike phase contrast.

The electric field immediately before the input pupil is given by

$$E(u, v) = P(u, v) \cdot A(1 + \varepsilon(u, v))e^{i\phi(u, v)} \quad (1)$$

where $P(u, v)$ is the pupil function, A is the mean electric field amplitude, $\varepsilon(u, v)$ is the point-by-point variation in the electric field strength, and $\phi(u, v)$ is the pupil-dependent phase. Assuming that $\phi(u, v)$ is small compared to a radian, the exponential term is Taylor expanded to first order. After all second order terms are dropped, the electric field is now given by

$$E(u, v) \approx P(u, v) \cdot A(1 + \varepsilon(u, v) + i\phi(u, v)). \quad (2)$$

The electric field at the pupil plane, given by Equation 2, is propagated to the image plane by a Fourier transform, represented by Equation 3:

$$E(\eta, \nu) = F[P(u, v)] * F[A(1 + \varepsilon(u, v) + i\phi(u, v))] \quad (3)$$

where $F[]$ represents the Fourier transform, the Cartesian coordinates at the image plane are given by η and ν , and the convolution is represented by the $*$ symbol. If the Fourier transform of the pupil function is represented by a point spread function, or PSF, and the Fourier transform of unity is represented by a delta function, Equation 3 is simplified to

$$E(\eta, \nu) = APSF(\eta, \nu) + APSF(\eta, \nu) * F[\varepsilon(u, v) + i\phi(u, v)]. \quad (4)$$

A uniform phase shift of magnitude θ is applied to the image plane PSF, giving a phase shifted electric field:

$$E(\eta, \nu) = APSF(\eta, \nu)e^{i\theta} + APSF(\eta, \nu) * F[\varepsilon(u, v) + i\phi(u, v)]. \quad (5)$$

Because the phase is imaged in the output pupil plane, Equation 5 is Fourier transformed to represent the electric field in the output pupil plane coordinates x and y :

$$E(x, y) = AP(x, y) \cdot (e^{i\theta} + \varepsilon(x, y) + i\phi(x, y)). \quad (6)$$

The re-imaged electric field represented in the output pupil by Equation 6 differs from the input pupil plane electric field in Equation 2 in that the DC part of the electric field, $(1 + \varepsilon(u, v) + i\phi(u, v))$, has been replaced by a phase shifted version, $(e^{i\theta} + \varepsilon(x, y) + i\phi(x, y))$.

Because the remaining expressions deal only with the output pupil plane, the explicit pupil notation $P(x, y)$ and coordinate notation are dropped.

If four different phase shifts between $\lambda/4$ and $\lambda/2$ ($\theta = -\pi/2, 0, \pi/2, \pi$) are introduced at the image plane, Equation 6 can be re-expressed as

$$\begin{aligned}
E_1 &= A(e^{-i\pi/2} + \varepsilon + i\varphi) = A(-i + \varepsilon + i\varphi) \\
E_2 &= A(e^{i0} + \varepsilon + i\varphi) = A(1 + \varepsilon + i\varphi) \\
E_3 &= A(e^{i\pi/2} + \varepsilon + i\varphi) = A(i + \varepsilon + i\varphi) \\
E_4 &= A(e^{-i\pi} + \varepsilon + i\varphi) = A(-1 + \varepsilon + i\varphi)
\end{aligned} \tag{7}$$

and their corresponding intensities as

$$\begin{aligned}
I_1 &= E_1 \cdot E_1^* = A^2(1 + \varepsilon^2 - 2\varphi + \varphi^2) \\
I_2 &= E_2 \cdot E_2^* = A^2(1 + \varepsilon^2 + 2\varepsilon + \varphi^2) \\
I_3 &= E_3 \cdot E_3^* = A^2(1 + \varepsilon^2 + 2\varphi + \varphi^2) \\
I_4 &= E_4 \cdot E_4^* = A^2(1 + \varepsilon^2 - 2\varepsilon + \varphi^2)
\end{aligned} \tag{8}$$

where E^* represents the complex conjugate of E . These four intensity measurements can be combined to estimate the phase and amplitude errors of the electric field at the input pupil:

$$\varphi = \frac{I_3 - I_1}{4A^2} \tag{9}$$

$$\varepsilon = \frac{I_2 - I_4}{4A^2} \tag{10}$$

Therefore, the phase and amplitude errors can be estimated by taking differences in the intensities measured at the output pupil (each intensity imaged corresponding to a different image plane phase shifts). The normalization term A^2 is calculated by propagating the electric field of the reference and science arms separately to the output pupil and multiplying the resulting intensities. The resulting A^2 term represents the amplitude of the electric field had no phase errors been introduced at the image plane.

3. EXPERIMENTAL SETUP

3.1 Testbed Overview

The purpose of the experimental testbed is to introduce and measure a known phase error. The testbed is shown schematically in Figure 2.

A red laser beam, soon to be replaced by a white light source, provides a narrow band input light source at the pupil plane. A microscope slide introduces a known phase error at the pupil plane. A Zygo interferometer measurement of the microscope slide phase provides a standard against which the Zernike phase measurement can be compared. Figure 3 shows the Zygo measurement of the testbed slide.

After passing through the microscope slide, the laser beam is propagated to the focal plane using a parabolic mirror. The focal plane assembly is composed of a single mode optical fiber inserted into a glass capillary tube. The end face of the filament is flush with the face of the capillary. The end faces of the filament and capillary are silver coated to act as mirrors. The filament is laterally shifted relative to the capillary using PZTs in order to phase shift the central $1.3\lambda/D$. The motion of the filament, or “reference arm,” therefore provides the phase shifts represented by the exponentials in Equations 7 and 8, while the unshifted light reflected by the capillary, or “science arm,” propagates to the Lyot pupil unchanged.

The shifted light reflected by the filament and the unshifted light reflected by the capillary is propagated to the Lyot pupil by a parabolic mirror. The recombined light is imaged by a pupil viewing CCD, resulting in the intensity measurements given by Equation 8.

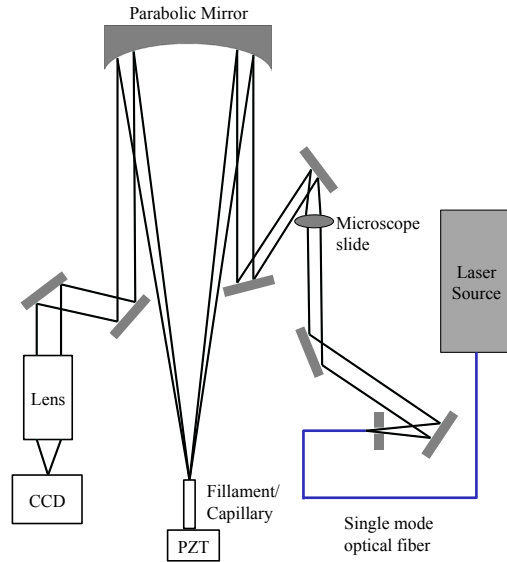


Figure 2. A schematic diagram of the ZWFS testbed.

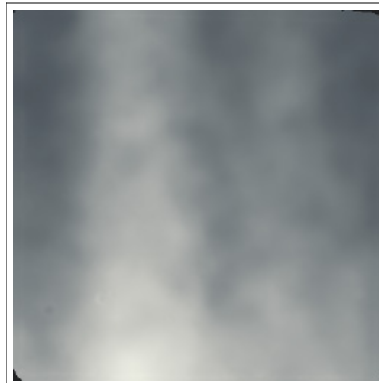


Figure 3. The phase errors introduced by a microscope slide, as measured by the Zygo interferometer.

3.2 Focal Plane Assembly

As described in Section 3.1, the image plane assembly consists of a glass capillary tube and a single mode fiber. The capillary has an outer diameter (OD) of 6 mm and an inner diameter (ID) of 126 μm . The fiber has a preliminary OD of 126 μm , etched in hydrofluoric acid to $\sim 123 \mu\text{m}$. The fiber is inserted into the capillary tube and cleaved using a fiber cleaver.

Initially, the fiber and capillary were assembled, coated, and integrated into the testbed without additional polishing of the off-the-shelf capillary tube. The resulting Lyot plane image, however, was divided into two light spots of different sizes, separated by about 2 cm. Zygo measurements of the assembly face show that the off-the-shelf capillary faces are tilted by about 10° relative to the optical axis, causing the separation reference arm and science arm beams the Lyot plane. Figure 4 shows the Zygo image of the tiled capillary face.

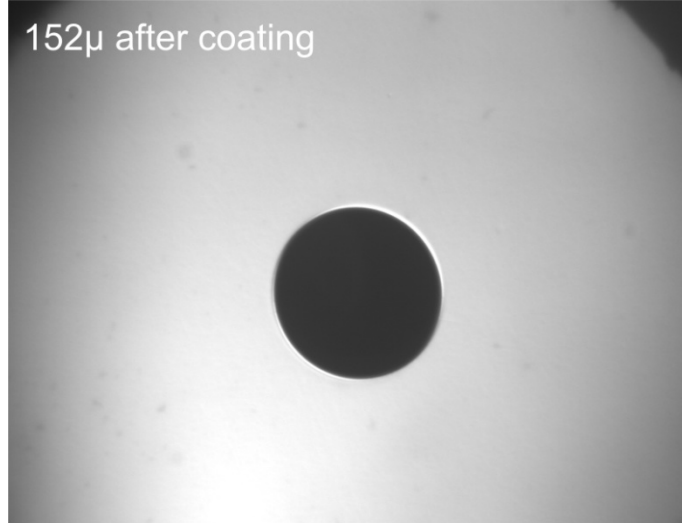


Figure 4. A photomicrograph of the end of the glass capillary after it has been polished and coated. This processing has left an excellent optical surface with flatness of 0.05λ P-V and the hole in the capillary well defined.

Further polishing of the capillary face is therefore necessary to overlap the beams reflected by the filament and capillary at the Lyot plane. We are currently pursuing methods of co-polishing the fiber and capillary faces with two different vendors, with a requirement that the capillary be polished to within 1.5 arcminutes of normal to the optical axis.

4. SIMULATIONS

4.1 Architecture

The purpose of the simulation is to compare the theoretical and lab performances of the Zernike wavefront sensor in order to identify and minimize sources of error in the lab.

The simulation imports the Zygo interferometer phase measurements of the same microscope slide used in the testbed (Figure 3). The piston, tip, and tilt errors are removed from the Zygo data using the first three Zernike polynomials. The phase errors are introduced into the uniform electric field at the input pupil, and the modified electric field is propagated to the image plane. At the image plane, a mask corresponding to the lab filament size is applied to the electric field. In this way, a phase shift is applied only to the region of light incident on the fiber portion of the image plane. The shifted and unshifted portions of the electric field are recombined at the Lyot pupil, where the intensities are used to calculate the phase (Equation 9). The electric field is propagated between the pupil and image planes using the semi-analytical method of Fourier transform.

4.2 Semi-Analytical Method of Fourier Transform

The Fourier transforms used to simulate the propagation of light between the pupil and image planes were calculated using the Semi-Analytical method (SAM) of Fourier transform. SAM provides a fast and memory efficient means of Fourier Transform between pupil and image planes in Lyot-style coronagraphs [1]. In order to represent small features of the optical system, both the pupil and image planes must be finely sampled, and the corresponding Fourier transform must be calculated at a very high frequency, creating demands on computer speed and memory efficiency. Unlike FFT methods, SAM removes the need for array padding, thus reducing the number of computations required to calculate the Fourier transform. By limiting the region of interest to a square array of side length N_A in the pupil plane and N_B in the image plane, the 2D FT of the function $f(X,Y)$ is computed by two matrix products:

$$F(U, H) = \frac{m}{N_A N_B} e^{-2i\pi UX^T} \cdot f(X, Y) \cdot e^{-2i\pi YV^T}$$

where m is N_B divided by the scale factor λ/D . The SAM and FFT methods yield numerically identical results over a range of input conditions, with a speed improvement of about factor of 35. Figure 5 compares the FFT and SAM methods at the input pupil, image plane, and output (Lyot) pupil.

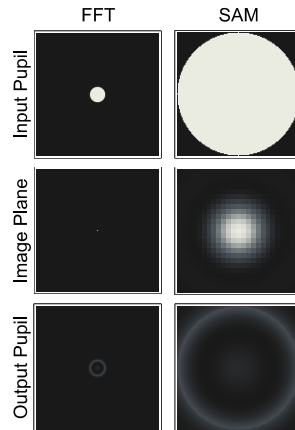


Figure 5. The results of the FFT and SAM methods are compared in the input pupil, image plane, and output pupil. Figure after Soummer et al 2007.

As a means of verifying the numerical accuracy of the two techniques, we devised the following method: given a sinusoidal input phase, the maximum intensity at the image plane and output pupil was calculated over a range of phase amplitudes using both the FFT and SAM methods. The methods agree exactly over the amplitude range sampled.

4.3 Simulation Results

The Lyot plane intensity measurements of the simulation are compared to the corresponding testbed measurements in Figure 6.

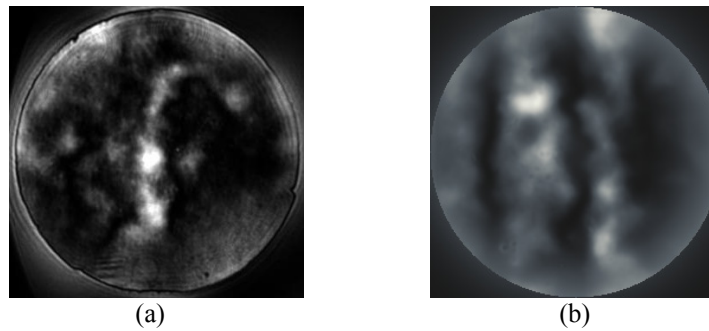


Figure 6. The intensity measured at the Lyot plane with phase errors introduced by a microscope slide in (a) the testbed and (b) the simulation. Both cases represent the “coronagraph mode,” in which the fiber is removed from the assembly, allowing only the light reflected by the capillary to propagate to the Lyot pupil.

The sensitivity of the simulation to both Fourier and Zernike modes was analyzed. In order to test the Fourier mode response, the phase reconstruction error was calculated as a function of sinusoidal input phase frequency for a range of phase amplitudes. The reconstruction error was quantified as the root mean square difference between the measured and actual phase amplitude. Figure 7 shows the results of this analysis.

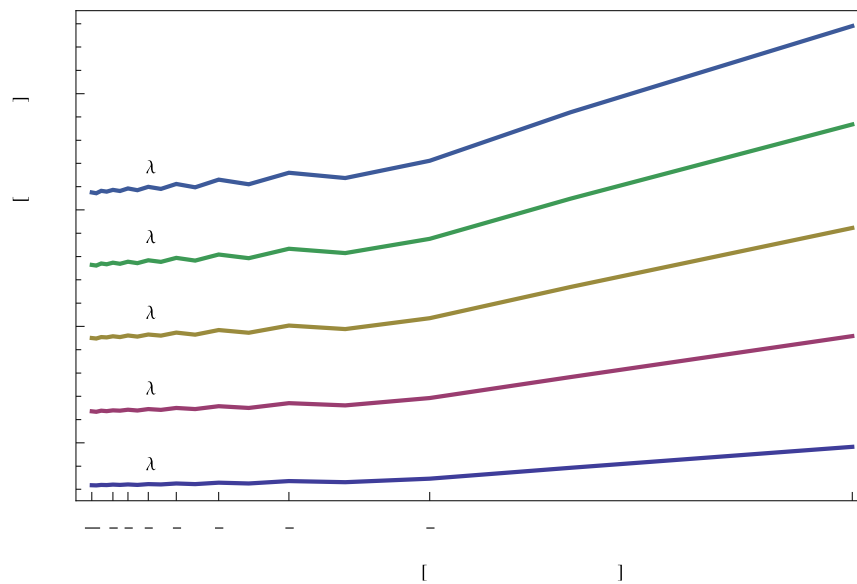


Figure 7. For a sinusoidal input phase, the root mean square difference between the measured and actual phase amplitude is plotted as a function of input phase frequency for input amplitudes of 0.1, 0.2, 0.3, 0.4, and 0.5 μm .

The sensitivity of the simulated wavefront sensor to the first fifty Zernike modes was calculated by varying each Zernike coefficient and calculating the corresponding change in reconstruction phase error. The results of this analysis are plotted in Figure 8.

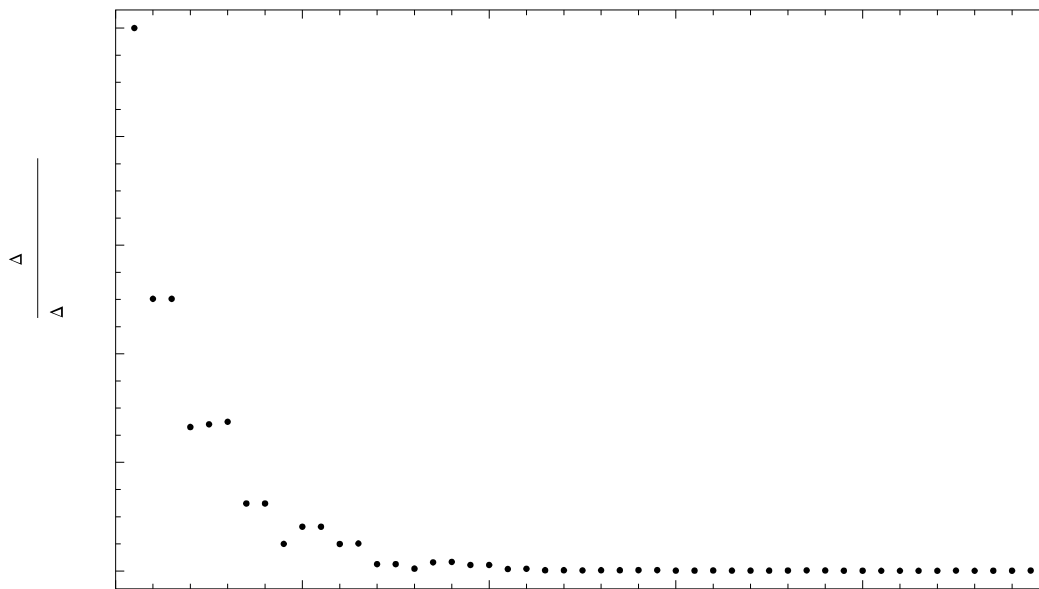


Figure 8. The change in reconstruction error divided by the change in Zernike term amplitude is plotted as a function of Zernike coefficient. The Zernike WFS is shown to be more sensitive to lower order aberrations, and very insensitive to higher order aberrations.

5. FUTURE PLANS

5.1 Testbed Validation

After acquiring a capillary tube polished to within 1° of normal to the optical axis, the testbed will be fully operational. The phase measurements of the testbed will be compared to those of the Zygo interferometer in order to validate the testbed performance. The testbed will be complete when the Zygo and testbed phase measurements agree to within 10 nm RMS.

5.2 Design and Fabrication of the Mount Palomar Adaptive Optics Wavefront Sensor

After demonstrating 10 nm RMS agreement between phase measurements with the lab testbed and Zygo interferometer, design and fabrication for the Mount Palomar AO Zernike wavefront sensor will begin. The Zernike sensor will be made to fit within the volume and weight restrictions placed by the Mount Palomar AO group. The Zernike sensor will be operational in 2013.

5.3 CCAT Segmented Mirror Phasing

6. ACKNOWLEDGEMENTS

This work was carried out by the Jet Propulsion Laboratory, California Institute of Technology, and was sponsored by the Space Grant Program and the National Aeronautics and Space Administration. This work was supported by JPL's Research and Technology Development Fund. We would like to acknowledge Rosemary Diaz for her support in fabricating the fibers and making the capillary/fiber assemblies, Victor White for his support in etching the bare fibers down to size, and Randy Bartos for his support in the opto/mechanical layout of the experiment as well as his design and fabrication of the custom mechanical components. We also thank our fine vendors: Nu-Tek for the polishing capabilities, and Coastline Inc. for the custom polishing and coating and for FiberGuide Industries for their fiber assemblies as well.

REFERENCES

- W. Linnik, "A simple interferometer to test optical systems," Proceedings of the Academy of Science of the USSR 1, 210-212 (1933).
- F. Zernike, "Das Phasenkontrastverfahren bei der Mikroskopischen beobachtung," Z. Tech. Phys. **16**, 454 (1935).
- Zernike, "Phasecontrast, a new method for the microscopic observation of transparent objects. Part I," Physica (Utrecht) **9** 686-698 (1942).
- F. Zernike, "Phasecontrast, a new method for the microscopic observation of transparent objects. Part II.," Physica (Utrecht) **9**, 974-986 (1942).
- F. Zernike, "How I discovered phase contrast," Science **121**, 345-349 (1955).
- J. W. Goodman, *Introduction to Fourier Optics* (McGraw-Hill, 1996).
- R. N. Smartt and W. H. Steel, "Theory and application of point-diffraction interferometers," Jpn. J. Appl. Phys. **14**, 351-356 (1975).
- E. E. Bloemhof, J. K. Wallace, "Simple broadband implementation of a phase contrast wavefront sensor for adaptive optics", Optics Express **12**, 6240 - 6245 (2004).
- M. A. Vorontsov , E. W. Justh, G. W. Carhart, L. A. Beresnev, Adaptive optics with advanced phase-contrast techniques. I. High-resolution wave-front sensing, J. Opt. Soc. Am. A **18**, 1289-1299 (2001).

- E. W. Justh, M. A. Vorontsov, G. W. Carhart, L. A. Beresnev, and P. S. Krishnaprasad, "Adaptive optics with advanced phase-contrast techniques. II. High-resolution wave-front control," *J. Opt. Soc. Am. A* **18**, 1300–1311 (2001).
- C. R. Mercer, K. Creath, "Liquid-crystal point-diffraction interferometer for wave-front measurements", *Appl. Opt.* **35**, pp. 1633, 1996
- G. E. Sommargren and R. Hostetler, "Point diffraction interferometry at soft x-ray wavelengths," in *Soft X-Ray Projection Lithography*, A. M. Hawryluk and R. H. Stulen, eds., Vol. 18 of OSA Proceedings Series 1 Optical Society of America, Washington, D.C., 1993, p. 10.
- G. E. Sommargren, "Phase shifting diffraction interferometry for measuring extreme ultraviolet optics," *OSA Trends in Optics and Photonics Vol. 4, Extreme Ultraviolet Lithography*, G.D. Kubiak and D.R. Kania, eds. (Optical Society of America, Washington, DC 1996), pp. 108-112.
- O. Guyon, "Limits of Adaptive Optics for High Contrast Imaging", *Astrophys. J.* **629** (2005), 592-614
- K. Dohlen, M. Langlois, P. Lanzoni, S. Mazzanti, A. Vigan, L. Montoya, E. Hernandez, M. Reyes, I. Surdej, N. Yaitskova, "ZEUS: a cophasing sensor based on the Zernike phase contrast method", *Proc. SPIE* **6267**, 626734 (2006).
- T. Huang, W. Lu, S. Zhang, A. H. Greenaway, "Zernike Phase Sensor for phasing of segmented telescopes", *Appl. Phys. B* **86**, 139-145 (2007).
- P. Ferraro, M. Paturzo and S. Grilli, "Optical wavefront measurement using a novel phase-shifting point-diffraction interferometer", *SPIE*